Neuro-Oncology
23(5), 732–742, 2021 | doi:10.1093/neuonc/noaa266 | Advance Access date 1 December 2020

Patient-derived orthotopic xenograft models of medulloblastoma lack a functional blood-brain barrier

Laura A. Genovesi,[†] Simon Puttick,[†] Amanda Millar, Marija Kojic, Pengxiang Ji, Anne K. Lagendijk, Caterina Brighi, Claudine S. Bonder, Christelle Adolphe, and Brandon J. Wainwright

The University of Queensland Diamantina Institute, Translational Research Institute, The University of Queensland, Woolloongabba, Queensland, Australia (L.A.G., A.M., M.K., P.J., C.A., B.J.W.); Institute for Molecular Bioscience, The University of Queensland, St Lucia, Queensland, Australia (L.A.G., A.K.L., B.J.W.); Probing Biosystems Future Science Platform, Commonwealth Scientific and Industrial Research Organization, Royal Brisbane and Women's Hospital, Brisbane, Queensland, Australia (S.P.); Australian Institute for Bioengineering and Nanotechnology, The University of Queensland, St Lucia, Queensland, Australia (C.B.); ARC Centre of Excellence in Convergent Bio-Nano Science and Technology, The University of Queensland, St Lucia, Queensland, Australia (C.B.); Centre for Cancer Biology, University of South Australia and SA Pathology, Adelaide, South Australia, Australia (C.S.B.); Adelaide Medical School, Faculty of Health Sciences, University of Adelaide, Adelaide, South Australia, Australia (C.S.B.)

Corresponding Author: Laura A. Genovesi, PhD, The University of Queensland Diamantina Institute, Translational Research Institute, The University of Queensland, 37 Kent Street, Woolloongabba, Queensland 4102, Australia (l.genovesi@uq.edu.au).

[†]These authors contributed equally to this work.

Abstract

Background. Novel targeted therapies for children diagnosed with medulloblastoma (MB), the most common malignant pediatric brain tumor, are urgently required. A major hurdle in the development of effective therapies is the impaired delivery of systemic therapies to tumor cells due to a specialized endothelial blood-brain barrier (BBB). Accordingly, the integrity of the BBB is an essential consideration in any preclinical model used for assessing novel therapeutics. This study sought to assess the functional integrity of the BBB in several preclinical mouse models of MB.

Methods. Dynamic contrast enhancement magnetic resonance imaging (MRI) was used to evaluate blood-brain-tumor barrier (BBTB) permeability in a murine genetically engineered mouse model (GEMM) of Sonic Hedgehog (SHH) MB, patient-derived orthotopic xenograft models of MB (SHH and Gp3), and orthotopic transplantation of GEMM tumor cells, enabling a comparison of the direct effects of transplantation on the integrity of the BBTB. Immunofluorescence analysis was performed to compare the structural and subcellular features of tumor-associated vasculature in all models.

Results. Contrast enhancement was observed in all transplantation models of MB. No contrast enhancement was observed in the GEMM despite significant tumor burden. Cellular analysis of BBTB integrity revealed aberrancies in all transplantation models, correlating to the varying levels of BBTB permeability observed by MRI in these models.

Conclusions. These results highlight functional differences in the integrity of the BBTB and tumor vessel phenotype between commonly utilized preclinical models of MB, with important implications for the preclinical evaluation of novel therapeutic agents for MB.

Key Points

1. Tumors from patient-derived orthotopic xenograft models of MB display regions of disrupted BBTB.
2. Tumors derived from our MCre:*Ptch1* SHH GEMM contain an entirely intact BBTB.
3. Structural vasculature defects correlate to varying levels of BBTB permeability.

Importance of the Study

Drug delivery across the BBTB is critical to the successful translation of novel therapies in neuro-oncology. Despite this, the functional status of the BBTB in preclinical models of MB remains largely unknown and is rarely considered in the preclinical assessment of novel agents. Here, we show for the first time that BBTB integrity is highly variable in preclinical models of MB raising questions as to the scope of the translational relevance of these models. Furthermore, we show variability in the cellular and molecular alterations underlying BBTB disruption and demonstrate that these differences correlate with imaging phenotypes derived from in vivo MRI. Our findings highlight the importance of characterizing the functional status of the BBTB in preclinical models of MB and we propose that these methods should be adopted more broadly in preclinical drug discovery for pediatric brain tumors.

Medulloblastoma (MB) represents the most common malignant pediatric brain tumor and the leading cause of cancer-related mortality and morbidity in children.[1] Four distinct molecular subgroups of MB have been defined, Wingless (WNT), Sonic Hedgehog (SHH), Group 3 (Gp3), and Group 4 (Gp4), with a number of subtypes across these groups more recently recognized.[2] Current standard-of-care treatment for average-risk patients results in 5-year survival rates of 70%–85% and <70% for high-risk patients,[1] dropping to less than 10% for children that relapse.[3] Patients that do survive suffer severe neuroendocrine-related side effects due to the intensive, cytotoxic nature of existing treatment protocols on the immature brain. Clearly, there is an urgent need to identify improved novel therapeutic strategies that are less toxic and more effective.

Preclinical mouse models play a central role in the discovery, development, and delivery of novel drug treatments, with the inherent assumption that preclinical efficacy of novel targeted therapies translates into clinically relevant outcomes. However, this can only be achieved if preclinical mouse models closely recapitulate the genetics and biology of the human disease.[4] Various murine models recapitulating each of the 4 MB molecular subgroups have been developed. Commonly used mouse models include predisposed germline, conditional inducible and transposon-based genetically engineered mouse models (GEMMs). Additionally, the field also employs orthotopic transplantation models using both mouse and human cell lines and patient-derived xenografts.[5] Each of these models has clear advantages and disadvantages. Genetically engineered mouse models play a fundamental role in addressing the tumor-forming potential of a given genetic mutation within a precise cellular lineage in the appropriate microenvironment and developmental setting. However, these models fail to represent the genetic heterogeneity or microenvironment of human tumors.[4] Tumors derived from patient-derived orthotopic xenograft (PDOX) models address these limitations, since they have been shown to maintain the characteristics of the human primary tumors from which they were derived.[6] Consequently, PDOX MB models are now widely used as the gold standard for preclinical testing of novel therapeutics.[7] Importantly, many of these preclinical studies in mice have led to clinical trials in children diagnosed with MB.

A major challenge for the discovery of novel therapeutics for pediatric brain tumors is the specialized vasculature comprising the blood-brain barrier (BBB). This selective and protective barrier functions to limit entry of potentially neurotoxic substances and pathogens into the brain.[8] The BBB is maintained by a multicellular structure called the neurovascular unit, consisting of highly specialized blood endothelial cells (ECs), pericytes, astrocytes, neurons, and extracellular matrix components.[8] Blood-brain barrier ECs are interconnected by highly continuous tight cell-cell junctions, lack fenestrations, and contain a low number of endocytotic vesicles.[8] As a result, transendothelial passage of substances from the blood to the brain is predominantly limited to the passive diffusion of substances with certain physiochemical properties. Alternatively, substances can cross by active regulation through major endothelial transport systems.[9] The nature of this physical and biochemical BBB represents a significant obstacle for the delivery of agents to tumors of the central nervous system. Ineffective delivery is thought to be partially responsible for the failure of novel therapeutic strategies in early phase clinical trials after demonstrating significant preclinical antitumor efficacy.[10] It is therefore imperative that preclinical MB models used for the assessment of drug efficacy are capable of accurately assessing and predicting if novel therapeutic agents can cross the BBB, thereby enhancing efficient translation into the clinic.

Disruption of the BBB is observed in a number of pathological conditions, including brain tumors. Cancer cells disrupt the connectivity between normal brain and ECs leading to a breakdown of the BBB and the formation of a blood-brain-tumor barrier (BBTB).[11] Clinically, BBB dysfunction in neurological neoplasms is commonly assessed by contrast-enhanced (CE) magnetic resonance imaging (MRI) using a gadolinium-based contrast agent.[12] Spatial heterogeneity in contrast enhancement is often observed[13] and contrast enhancing regions and nonenhancing regions have been shown to exhibit significantly different histopathology.[14] Sonic Hedgehog and Gp3 MB patients present with heterogeneous enhancement patterns, whereas minimal or nonenhancing tumors are characteristic of Gp4 MB.[15,16] The degree to which these clinical observations of BBB integrity are recapitulated in the wide array of preclinical mouse models for this disease remains to be determined. To date, the use of high-resolution MRI to interrogate the functionality of the BBTB in murine models of MB is extremely limited. Blood-brain-tumor barrier integrity has been

examined on the basis of MRI for only one mouse model of MB. In this study, the majority of the tumors generated in the *Smoothened* homozygous (*Smo:Smo)* GEMM of the SHH subgroup maintained an intact BBTB.[17] A subsequent study utilizing dextran leakage as a measure of vessel permeability identified a compromised BBTB following orthotopic transplantation of mouse in WNT (mWNT) but not mouse SHH (mSHH) tumors from various GEMMs.[18] Given PDOX models are the most frequently used models for the preclinical evaluation of novel therapeutics, the paucity of high-quality preclinical data on the status of the BBTB remains of interest.

Here, we use high-resolution MRI to interrogate the integrity and permeability of the BBTB in several preclinical models of MB. Subsequent pharmacokinetic (PK) modeling of dynamic contrast-enhanced (DCE) MRI data was used to derive the rate constant defining the transfer of contrast agents from the vascular lumen to the extravascular space (K^{trans}).[19] We investigate the structural and cellular features of the blood vasculature in Math1Cre-driven *Patched1* (MCre:*Ptch1*) SHH GEMM tumors (homozygous inactivation of *Ptch1* in MCre-derived granule neuron progenitors of the cerebellum), in an orthotopic transplantation model of the MCre:*Ptch1* SHH GEMM tumors (Ortho-MCre:*Ptch1*), and in both SHH and Gp3 PDOX tumors. We subsequently correlate trends in the kinetics of contrast enhancement observed in each tumor model to the morphology of cell-cell junctions in the vasculature and to the expression of plasmalemma vesicle-associated protein (Plvap), a key component of stomatal and fenestral diaphragms.[20] Our data indicate that the function and organization of vascular networks are not only significantly different between distinct molecular subgroups of MB, but that the process of engraftment also compromises BBTB integrity. Furthermore, we show that differences in contrast enhancement patterns and the kinetics of contrast agent uptake in the tumor assessed by DCE MRI correlates with both the organization of tumor vasculature and with molecular differences in the BBTB.

Methods

Mice

All experimentation was reviewed and approved by The University of Queensland Molecular Biosciences animal ethics committee. Six- to 10-week-old NOD.Cg-Prkdc^{scid} Il2rg^{tm1Wjl}/SzJ (NSG) mice were originally purchased from The Jackson Laboratory (Bar Harbor, ME) and maintained as a colony at the Translational Research Institute, University of Queensland. Mice with granule neuron progenitor-specific deletion of Ptch1 were generated by breeding animals carrying the conditional *Ptch1* (*Ptch1*$^{Lox/Lox}$)[21] with Math1Cre (*Math1*^{Cre}) transgenic mice.[22] Experiments described in this study were conducted on 4 groups of mice designated: MCre:*Ptch1* (n = 5), SHH PDOX (n = 3), GP3 PDOX (n = 3), and Ortho-MCre:*Ptch1* (n = 3).

Orthotopic GEMM and PDOX Transplantation Models of MB

Studies were conducted using orthotopic transplantation of tumor cells derived from MCre:*Ptch1* mice, Med-411FH, and Med-1712FH PDOX models. Med-411FH and Med-1712FH were generated in the Olson Laboratory (Fred Hutchinson Cancer Research Center, Seattle) using pediatric patient tumor tissue obtained from Seattle Children's Hospital with approval from the Institutional Review Board. Med-411FH is a *MYC*-amplified Gp3 MB with large cell/anaplastic morphology that was derived from a 3-year-old male patient. Med-1712FH is a SHH MB with desmoplastic/nodular morphology, derived from a 4.9-year-old patient. Patient-derived orthotopic xenograft lines were established and propagated as previously described and genomic analysis performed to compare to primary tumors from which they originated.[6,7] To generate the ortho-MCre:*Ptch1* model, tumors from MCre:*Ptch1* were harvested and immediately processed for orthotopic transplantation into NSG mice. Tissue was processed as per standard protocol using enzymes from brain tumor dissociation kit ((P) 130-095-942), with this single cell suspension filtered, centrifuged, and resuspended in serum-free Dulbecco's modified Eagle's medium to a concentration of 1×10^6 cells/μL. Two microliters of the cell suspension (2×10^6) cells was injected into NSG mice using the exact protocol as PDOX tumors.[7]

MRI Acquisition and Image Analysis

Mice were imaged on a Bruker 7T ClinScan fitted with a 23-mm volume coil. A cannula preloaded with Gadovist (100 μL,0.2 mmol/mL) was placed in the tail vein. Imaging sequences included a 3D DIXON-VIBE image (repetition time [TR] = 12 s, echo time [TE] = 1.78 s, fractional anisotropy [FA] = 4° and 21°, 0.12 mm isotropic resolution) followed by a series of 2D sagittal T_2 weighted slices (TSE, TR = 4372 s, TE = 45 s, slice thickness = 0.7 mm, in-plane resolution = 0.08 mm) and a series of 80 DCE images (3D VIBE, TR = 10 s, TE = 0.93 s, FA = 21°, slice thickness = 0.63 mm, in-plane resolution = 0.195 mm, temporal resolution = 8 s) prior, during, and postinjection of Gadovist. Finally, the 3D VIBE image was repeated to obtain a T_1 weighted CE image. All images were first coregistered to a precontrast 3D T_1 weighted image using affine transformation only and T_2 enhancing volume was manually segmented for each mouse. This volume was transformed onto DCE parametric maps for calculation of mean PK parameters. For MCre:*Ptch1* mice where T_2 enhancement was minimal, the whole cerebellum was segmented.

DCE MRI Analysis

Pharmacokinetic analysis of DCE MRI images was performed on an image series of 80 T_1 weighted transverse images acquired before, during, and after contrast agent injection. The parameters K^{trans} and V_e were calculated on a voxel-wise basis using an extended Tofts 3-parameter

model (see Supplementary Material for details). For comparison between groups, parametric maps were registered to the T_1 weighted precontrast image and segmented volumes were applied to parametric maps to extract values of mean K^{trans} and V_e.

Immunohistochemistry and Immunofluorescence Analysis of Tumors

Antibody markers were analyzed on 7 micron, paraffin-embedded sections via standard immunofluorescence techniques using the following antibodies: PLVAP (BD Biosciences #553849, 10 μg/mL), CD31 (Abcam #28364, 1:50), Glucose transporter 1 (Glut1) (Merck #07-1401, 10 μg/mL), Glial fibrillary acidic protein (GFAP) (Merck #MAB360, 1:100), Claudin 5 (CLDN5) (Abcam #131259, 1:100), and human mitochondria (huMITO) (Merck #MAB1273, 1:50). AF594-labelled donkey anti-rabbit or AF488 donkey anti-rat or anti-mouse (1:250, Invitrogen) secondary antibodies were used and sections counterstained with DAPI (Sigma Aldrich). Images were captured using Zeiss Axiovert 200 confocal microscope with LSM 710 scanner with presented as the sum of the Z-stack projection. Immunohistochemistry analysis was performed using the following primary antibodies: carbonic anhydrase IX (CAIX) (Creative Biolabs, #PABZ-017), hypoxia-inducible factor 1 subunit α (HIF1α) (Novus Biologicals, #NB100-449), and anti-CD31 antibody (1:1000, Santa Cruz Biotechnology, Dallas, TX). Images were obtained using Olympus BX-51 microscope. For all stains, 3 sections from each mouse were analyzed per model, with a total of 3 mice per model assessed. Staining was visualized using Vectastain Elite ABC and ImmPACT DAB (Vector Laboratories, Burlingame, CA). The CD31-stained sections were further stained using a periodic acid-Schiff (PAS) staining kit from Merck Millipore (Burlington, MA) according to manufacturer's instructions. Stained sections were scanned by the whole slide image (WSI) scanner (Hamamatsu NanoZoomer Slide scanner). All slides were de-identified prior to scoring and tumor vasculature was manually counted with the EC-lined blood vessels ($CD31^+PAS+$) and VM structures ($CD31^-PAS+$) confirmed by the presence of RBCs or WBCs within the lumen. As tumor sizes varied, the number of fields of view (FsOV) available for analysis differed with 3–9 FOV available per tumor. To quantify the density of VM networks, a 1–4 scoring system was undertaken of the colorimetric PAS reaction for each of the de-identified tumor sections, with 4 representing the highest PAS+ network within a section. Fluorescence emission from PAS staining was photographed on a Zeiss LSM 710NLO microscope.

In Silico Promoter Screening

The minimal HIF binding consensus sequence RCGTG was obtained from.[23] The PLVAP promoter sequence up to the transcription start site (TSS) was downloaded from the Ensembl database[24] and screened for the presence of the RCGTG sequence using MacVector DNA Analysis Software package (version 12.7.4).

Results

Orthotopic Transplantation Models of MB Lack a Functional BBTB

To investigate the integrity of the BBTB, we acquired a combination of structural MR images as a proxy for vascular integrity, including CE T_1 and T_2 weighted images. Contrast-enhanced T_1 weighted images acquired after injection of gadolinium-based contrast agents are used to define the tumor mass characterized by a disrupted BBTB, as the extravasation of contrast agent occurs only in compromised vasculature.[25] T_2 weighted images acquired prior to contrast agent injection are used to characterize the entire tumor volume, comprehensive of vasogenic edema caused by nonenhancing infiltrating tumor with an intact BBTB, which is defined by regions of signal hyperintensity caused by reactive changes in the tumor microenvironment.[25] Visual comparisons of coregistered T_2 weighted images and CE T_1 weighted images show a dramatic difference between tumors originating from (1) MCre:*Ptch1* SHH mice (Figure 1A, E, and I), (2) SHH PDOX (Figure 1B, F, and J), (3) GP3 PDOX (Figure 1C, G, and K), and (4) ortho-MCre:*Ptch1* SHH tumors (Figure 1D, H, and L). Both SHH PDOX and Gp3 PDOX show significant contrast enhancement across the majority of the tumor volume (Figure 1I and J). The invasive front of SHH PDOX tumors show minimal contrast enhancement (yellow arrow, Figure 1F and J), indicating that in this model there is a difference in vascular integrity where tumor tissue meets the brain parenchyma. In contrast, MCre:*Ptch1* tumors display no contrast enhancement across the entire tumor volume despite significant tumor burden, indicating that MCre:*Ptch1* tumors exhibit a fully functional BBTB. However, upon orthotopic transplantation of these tumors, referred to as ortho-MCre:*Ptch1*, the entire tumor mass presents with contrast enhancement. To ensure that the surgical procedure itself did not result in the same imaging phenotype, we performed intracranial injections of the matrigel solution alone in mice and acquired MR images 2 weeks postsurgery. No contrast enhancement was observed in this group of mice (Supplementary Figure 1), indicating that the surgical procedure alone is not responsible for breakdown of the BBTB. Taken together, these data indicate that distinct biological processes govern tumor vascularization in tumors that initiate endogenously compared to orthotopic tumor cell engraftment in an host mouse. Therefore, our data indicate that the process of orthotopic transplantation to generate a tumor leads to defective vasculature and BBTB permeability.

Gp3 PDOX and Ortho-MCre:Ptch1 SHH Tumors Display Greater BBTB Disruption Than an SHH PDOX Model of MB

To further investigate the functionality of the BBTB in each model, we performed PK analysis on a series of T_1 weighted MR images acquired dynamically during uptake of Gadovist.

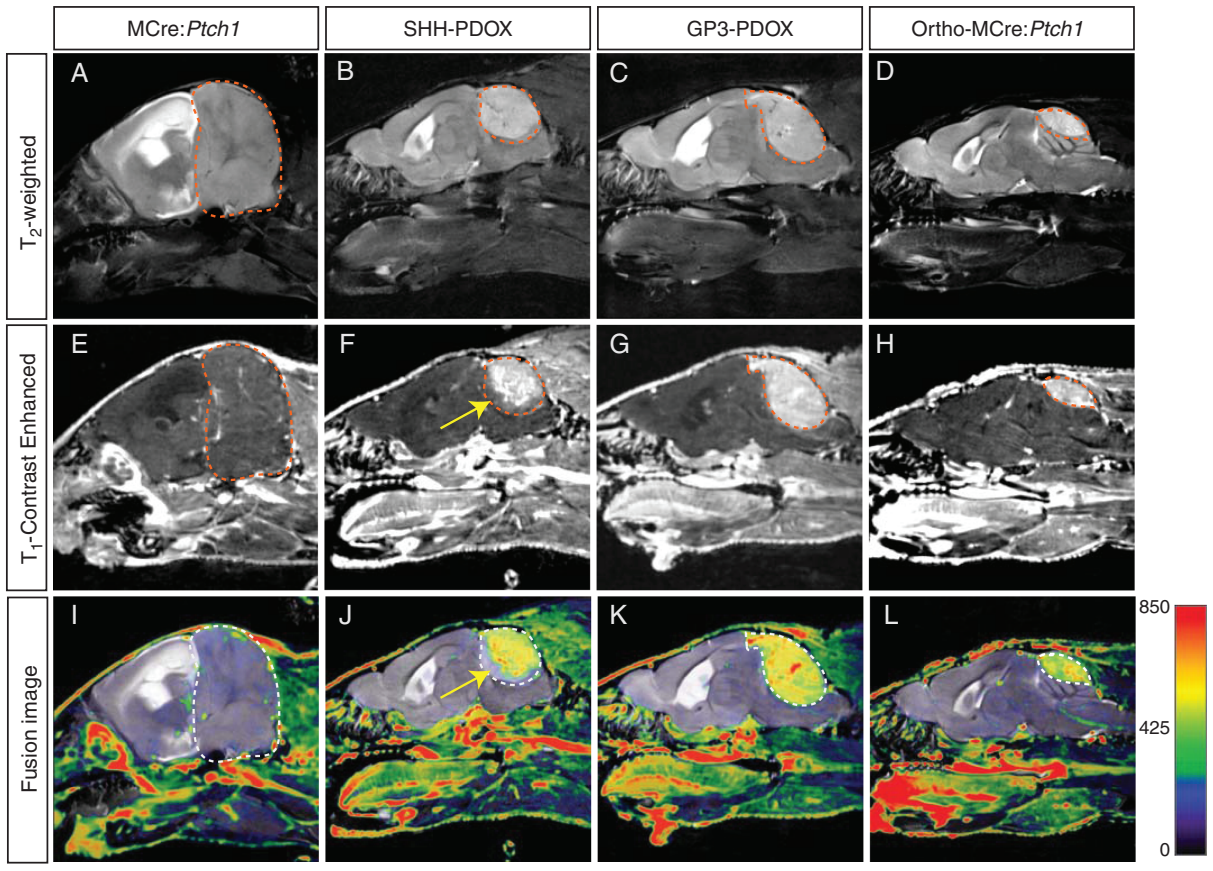

Fig. 1 Contrast-enhanced MRI phenotype in tumors derived from murine, PDOX, and allograft models of MB. Representative T_2 weighted and T_1 weighted contrast-enhanced MR images and coregistered fusion images in MCre:Ptch1 (A, E, I), SHH PDOX (B, F, J), Gp3 PDOX (C, G, K), and ortho-MCre:Ptch1 (D, H, L). Tumor volumes are outlined in red dashed lines (A–H) and white dashed lines (I–L). A region of noncontrast enhancing tumor in SHH PDOX mice is highlighted by the yellow arrows (F and J). MB, medulloblastoma; MRI, magnetic resonance imaging; PDOX, patient-derived orthotopic xenograft; SHH, Sonic Hedgehog.

Uptake curves for each of the models are distinctly different leading to different trends in PK parameters, indicating subtle differences in the mechanism of BBTB dysfunction (Figure 2E–H). More detailed analysis revealed that the SHH PDOX model is characterized by a gradual uptake of contrast agent with no peak during the imaging window. The Gp3 PDOX and Ortho-MCre:*Ptch1* models however both show a rapid uptake phase followed by steady decrease in longitudinal signal relaxation rate (R1). This is reflected in the higher value of K^{trans} [26] for both of these models (Figure 2I). These data indicate that the transfer of contrast agent from circulation to tissue occurs more rapidly, potentially indicating a different mechanism of transport in these 2 models. Additionally, the rate of decrease in R1 is faster in the ortho-MCre:*Ptch1* model than in the Gp3 PDOX, indicating that the retention of contrast agent in the ortho-MCre:*Ptch1* tumor tissue is greater in the Gp3 PDOX. This is reflected in the lower value of V_e [26] in the ortho-MCre:*Ptch1* model (Figure 2J). These distinct signatures in the kinetics of contrast agent uptake indicate subtle differences in the permeability of the vasculature and prompted us to investigate vascular characteristics on a molecular level.

Disorganized EC-Cell Junctions Are a Hallmark of BBTB Disruption in Orthotopically Transplanted MB Models

Histological analysis of brain tumor sections revealed vessel-like structures of varied size and shape (Figure 3A–D). To quantify newly formed tumor vasculature that sprouted from existing blood vessels through angiogenesis, tissue sections were stained with EC-specific marker, anti-CD31/PECAM-1, and PAS which stains basement membranes rich in collagen and laminin.[27] Tumor vasculature devoid of an EC lining (CD31-) has been previously characterized as vasculogenic mimicry (VM), whereby cancer cells mimic ECs to form their own vascular structures.[28] Supplementary Figure 2A exemplifies the closed loops of (1) $CD31^+PAS+$ vessels formed by angiogenesis and (2) $CD31^-PAS+$ VM detectable in MB. Blinded analysis of tumor vasculature in the 4 tumor groups indicated increased angiogenesis (Supplementary Figure 2B) and increased VM (Supplementary Figure 2C) in all orthotopic transplantation tumors. We observed a significant increase in the PAS+ VM network score in the

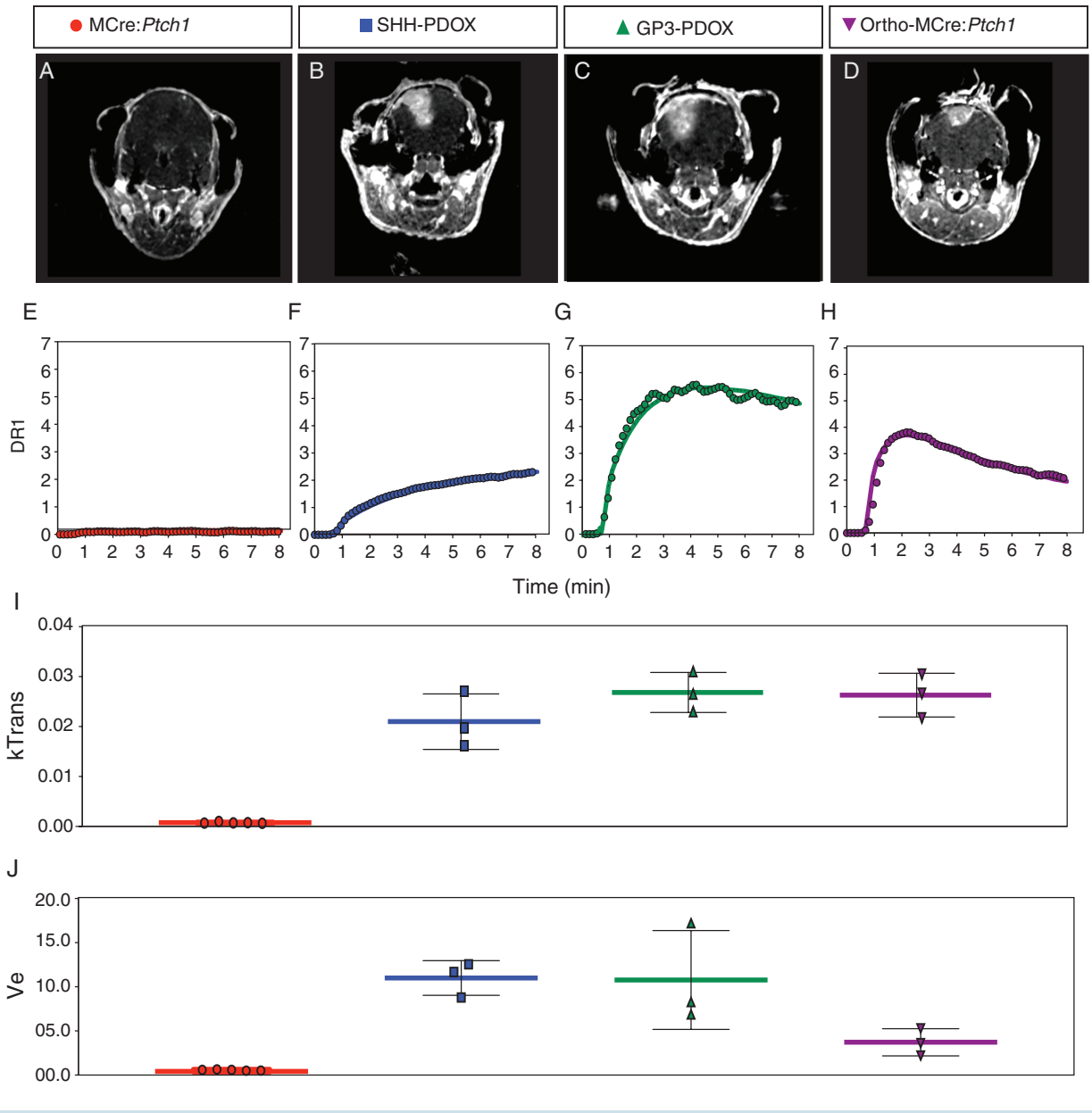

Fig. 2 Dynamic contrast-enhanced (DCE) MRI phenotype in tumors derived from PDOX and allograft models of MB. Representative transverse contrast-enhanced MRI slices (A–D) used for PK modeling of contrast agent uptake; representative enhancement signal (symbols) and model fits (solid line) in MCre:Ptch1 (E), SHH PDOX (F), Gp3 PDOX (G), and ortho-MCre:Ptch1 (H) and derived mean K^{trans} (I) and mean V_e (J) values. MB, medulloblastoma; MRI, magnetic resonance imaging; PDOX, patient-derived orthotopic xenograft; PK, pharmacokinetic; SHH, Sonic Hedgehog.

MCre:*Ptch1* tumors above all others, suggesting denser extracellular matrix and thus more rigid vessel environment (Supplementary Figure 2D).

Adhesion molecule CD31 resides at cell-cell junctions of ECs and is known to regulate junctional integrity of the BBB.[29] We therefore assessed the junctional localization of CD31 and observed that MCre:*Ptch1* tumors exhibit an organized, linear expression of CD31, clearly outlining a continuous vessel structure (Figure 3E). In contrast, diffuse, irregular, and punctate CD31 staining was observed in the SHH PDOX (Figure 3F), Gp3 PDOX (Figure 3G), and ortho-MCre:*Ptch1* tumors (Figure 3H). We also observed focal loss of EC CD31 expression which is characteristic of "mosaic tumor vessels," previously identified in colon carcinoma PDOX models[30] and linked to tumor vessel leakiness.[31] These findings were confirmed on the basis of an additional EC tight junction protein critical to maintaining BBB integrity, CLDN5 (Supplementary Figure 3).[9] Astrocytes maintain BBB integrity by secreting factors that upregulate tight junction protein expression in ECs of the BBB.[8] Therefore, differences in the expression of EC junctional markers

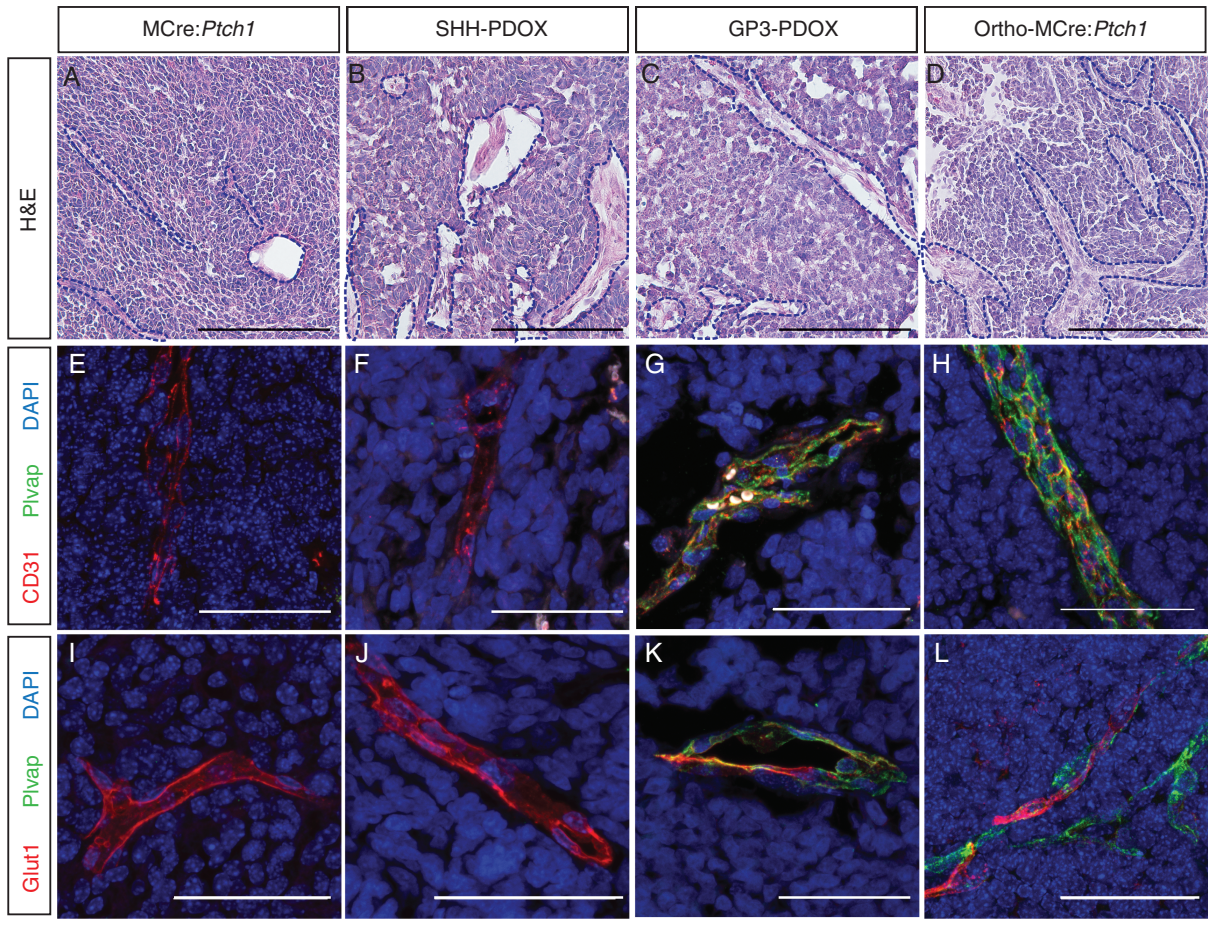

Fig. 3 Vessel phenotype in tumors derived from murine, orthotopic PDOX, and allograft models of MB. Representative H&E and co-immunofluorescence microscopy of CD31 (red), Plvap (green), and Glut1 (red) costained with DAPI (blue) in MCre:Ptch1 (A, E, I), SHH PDOX (B, F, J), Gp3 PDOX (C, G, K), and ortho-MCre:Ptch1 (D, H, L). All images were acquired at ×80 total magnification. Scale bars: 50 μm. Blood vessels are outlined with a blue dashed line. MB, medulloblastoma; PDOX, patient-derived orthotopic xenograft; SHH, Sonic Hedgehog.

could reflect variations of these cells within the NVN. CLDN5-expressing tumor vessels were devoid of astrocytes within SHH PDOX and Gp3 PDOX, with minimal astrocytic coverage of CLDN5-expressing vessels observed in ortho-MCre:*Ptch1* tumor (Supplementary Figure 3). In contrast, extensive astrocytic encircling of CLDN5-expressing vessels was observed within MCre:*Ptch1* tumors (Supplementary Figure 3). Diffuse, irregular CD31 and CLDN5 expression in all orthotopic transplantation models of MB strongly suggest that defects in intercellular adhesion between ECs contribute to the focal paracellular, hyperpermeability of tumor vessels and the lack of a functional BBTB in all orthotopic transplantation models irrespective of subgroup.

Gp3 and Ortho-MCre:Ptch1 PDOX Models Develop Fenestrated Tumor Vessels Resulting in a Compromised Barrier

To further investigate why Gp3 PDOX MB and Ortho-MCre:*Ptch1* SHH MB tumors display a greater BBTB disruption than other models, we next assessed the subcellular expression of proteins that are essential for BBB integrity. Plvap is an EC-specific structural protein necessary for fenestrated endothelium and is normally expressed in primitive vasculature prior to the induction of BBB properties and in tumor vessels undergoing angiogenesis.[9,20] Immunofluorescence analysis identified that all tumor models contain CD31^{+}/Plvap– vessels, characteristic of intact BBB. In Gp3 PDOX and ortho-MCre:*Ptch1* SHH tumors, we also identified a proportion of CD31^{+}/Plvap+ vessels (Figure 3G and H). CD31^{+}/Plvap+ vessels which were largely confined to the central region of the tumor mass (Supplementary Figure 4). Counterstaining with a human-specific mitochondrial antibody confirmed that CD31^{+}/Plvap+ vessels within Gp3 PDOX tumors were of murine origin (Plvap+/huMITO–) (Supplementary Figure 5). Given fenestrae act as physical sieves controlling the transendothelial exchange of molecules, these data indicate that CD31^{+}/Plvap+ vessels likely contribute to transcellular leakage of systemically administered compounds from blood to tissue. These findings are consistent

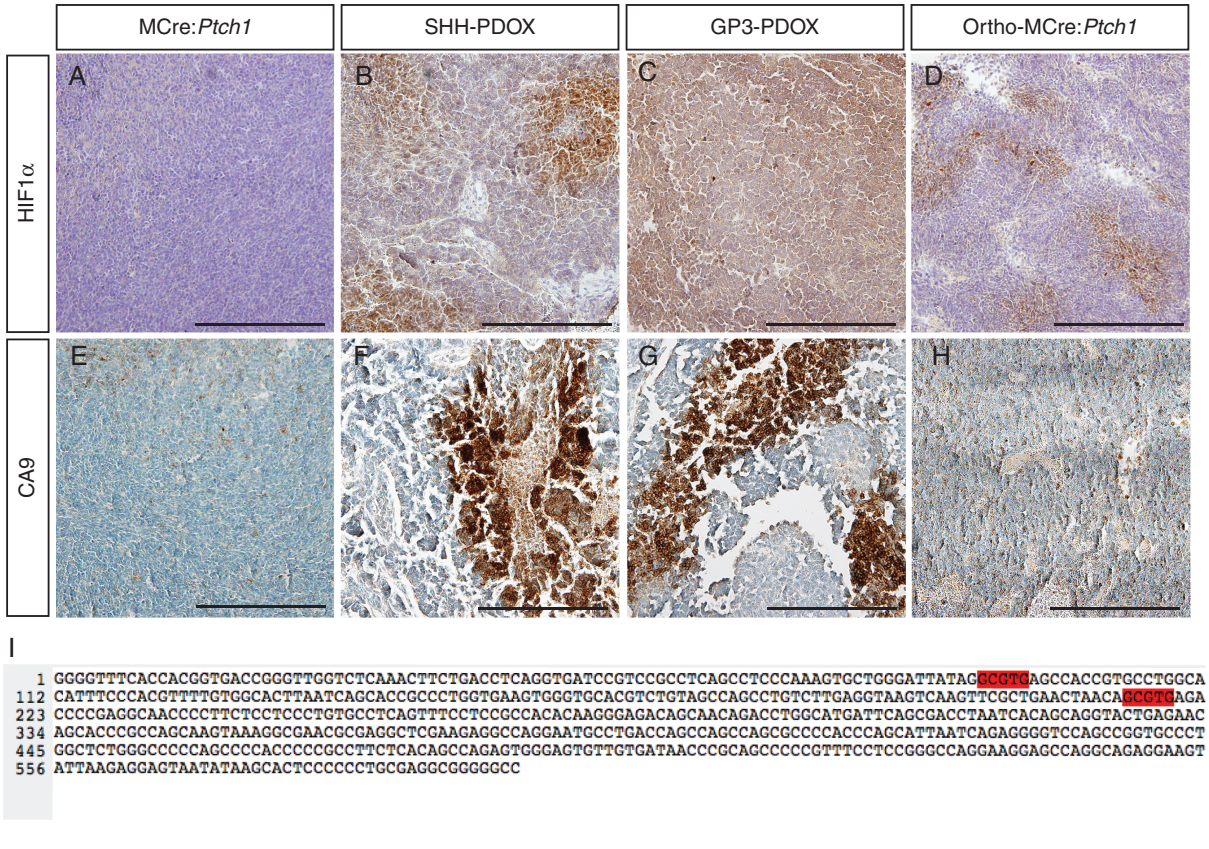

Fig. 4 Markers of hypoxia are associated with all orthotopically transplanted models of MB. Representative IHC microscopy of HIF1α and CAIX in MCre:Ptch1 (A, E), SHH PDOX (B, F), Gp3 PDOX (C, G), and ortho-MCre:Ptch1 (D, H). All images were acquired at ×20 total magnification. Scale bars: 200 μm. Hypoxia-inducible factor 1 α binding sites within the promoter sequence of *PLVAP* (I). CAIX, carbonic anhydrase IX; HIF1α, hypoxia-inducible factor 1 subunit α; IHC, immunohistochemistry; MB, medulloblastoma; PDOX, patient-derived orthotopic xenograft; SHH, Sonic Hedgehog.

with the distinct differences in the kinetics of uptake of MR contrast agent we identified when comparing the SHH PDOX and Gp3 PDOX and ortho-MCre:*Ptch1* SHH tumors.

Given that Plvap is repressed during BBB induction,[32] we next examined vascular expression of Glucose transporter 1 (Glut1). Glucose transporter 1 is a major glucose transporter in the mammalian BBB crucial to the induction of the barrier properties a mature BBB.[9] While tumors from all 4 models contained vessels with a Glut1+/Plvap– BBB-like vasculature (Figure 3M and N), the ortho-MCre:*Ptch1* and Gp3 PDOX tumors also contained vessels with regions of immature Glut1–/Plvap+ vasculature (Figure 3O and P). Together, the presence of Plvap and concomitant absence of Glut1 absence in the tumor-associated vasculature of ortho-MCre:*Ptch1* and Gp3 PDOX MB models indicates a failure to establish a specialized BBB in these models.

Elevated Levels of Hypoxic Markers Correlate to Vascular Defects in All Orthotopic Transplantation Models of MB

Intratumoral hypoxia is a well-known driver of neovascularization, resulting in the formation of disorganized, tortuous, and leaky vasculature.[33] On this basis, we next asked whether hypoxia contributed to the various vascular defects observed across all orthotopic transplantation models by examining HIF1α expression, a well-known marker of cellular hypoxia. Hypoxia-inducible factor 1 α-positive regions were observed throughout SHH PDOX (Figure 4B), Gp3 PDOX (Figure 4C), and ortho-MCre:*Ptch1* SHH tumors (Figure 4D), with focally intense regions observed in both the SHH PDOX and ortho-MCre:*Ptch1* SHH tumors. In contrast, HIF1α expression was not detectable in MCre:*Ptch1* tumors (Figure 4A). In agreement with these observations, we identified intense focal staining for CAIX, an important mediator of hypoxia and downstream target gene of HIF1α,[34] in SHH (Figure 4F) and Gp3 PDOX (Figure 4G), and a more moderate staining pattern in ortho-MCre:*Ptch1* SHH tumors (Figure 4H). Consistent with the HIF1α staining, CAIX staining was completely absent in tumors from MCre:*Ptch1* tumors (Figure 4E). These data indicate that upregulation of hypoxia-related markers is positively correlated to the extent of BBTB disruption across our models. To evaluate whether HIF1α might be directly regulating structural proteins of leaky endothelium, the *PLVAP* promoter around the TSS was scanned for the presence of the minimal HIF binding consensus sequence

RCGTG.[23] We identified 2 potential HRE sites within this region, 506 and 381 nucleotides (nt) upstream of the TSS of *PLVAP* (Figure 4I). Taken together, our data suggests that hypoxia might be the driving factor initiating the formation of aberrant, dysfunctional vasculature in all orthotopic transplantation models. The absence of hypoxia in tumors from MCre:*Ptch1* mice is likely due to coevolution of tumor cell proliferation with vascularization at a rate that maintains tissue normoxia, facilitating the formation of functional intact vasculature.

Discussion

New targeted therapies are urgently needed for children diagnosed with MB. However, the development of novel therapeutics is met with several challenges, including the very high attrition rate of candidate anticancer agents in clinical trial. The fundamental disconnect between the efficacy of anticancer agents observed in preclinical models and translation into clinical efficacy is well recognized, with only 5% of new agents entering clinical trial displaying sufficient activity to ultimately lead to licensing.[35] Hence, there is mounting pressure for (1) extensive testing employing representative preclinical models that are more predictive of the clinical setting and (2) defining outcome measures that are informative of treatment efficacy. Magnetic resonance imaging offers a wide diversity of contrast mechanisms ideally suited to intracranial neoplasms, allowing measurement of BBTB breakdown in a noninvasive and longitudinal manner.[15,16] This is the first study to use high-resolution CE and DCE MRI to interrogate the integrity and permeability of the BBTB and correlate this to structural features of tumor-associated vasculature in preclinical models of MB. Our data highlight the importance of considering the BBTB in assessing the clinical efficacy of novel therapeutic agents in preclinical studies for MB, thereby ensuring only clinically effective drugs enter trial.

Failure to appropriately treat and deliver therapeutics to all regions of the tumor, including those protected by an intact BBTB, results in residual disease following therapy and likely acts as the source of recurrence.[36,37] Comprehensive analysis of patterns of tumor recurrence has identified approximately 30% of all relapse patients as presenting with local relapse, with SHH tumors in particular largely recurring in the local tumor bed.[38] Undoubtedly, local relapse is partly a consequence of failure to deliver therapy to the entire primary tumor mass. Clinical MR gadolinium-based imaging studies have failed to identify the entire tumor margin in patients diagnosed with Gp3 and SHH MB, largely due to infiltrating tumor cells residing within an intact BBTB which remain undetectable by this method of imaging.[15,16] These findings have significant implications for anti-tumor treatment efficacy, as these undetectable regions are not resected by MRI-assisted surgery and are also protected from the delivery of therapeutics that do not penetrate the BBTB. Indeed, previous studies have shown that therapeutic sensitivity and favorable patient prognosis correlates to the presence of a disrupted BBB.[18] Therefore, in order to make significant progress in eradicating MB, particularly those diagnosed with recurrent MB which is almost universally fatal,[38] it is imperative to move forward with clinical therapeutic agents that are effective at crossing intact vasculature.

The extent of the heterogeneity of vasculature within MB not well defined. Elevated vascular endothelial growth factor (*VEGF*), a principal angiogenic factor,[39] was identified in cell line based xenograft Gp3 models and patients with Gp3 MB relative to other molecular subgroups, suggesting a role for angiogenesis in this subgroup.[40] Tumor neovascularization not only occurs through angiogenesis, but a number of additional mechanisms including VM, transdifferentiation of tumor cells into tumor ECs, and vessel co-option.[39] The identification of $CD31^{+}PAS-$ and $CD31^{-}PAS+$ vessels imply that both angiogenesis and VM contribute to tumor vascularization in preclinical models of both SHH and Gp3 MB. VM has been identified in 22% of MB patients and was associated with reduced survival.[41] Antiangiogenic agents have no effect on VM[42] and have been shown to induce VM formation,[43,44] raising questions to the appropriateness of targeting angiogenic pathways in MB. Importantly, phase II clinical trials investigating the survival benefit of Bevacizumab in combination with chemotherapy in pediatric patients diagnosed with recurrent MB are currently underway (NCT01217437 and NCT01356290). Our data reveal that these studies should be interpreted with caution and that further characterization of tumor vasculature within MB is necessary to guide both angiogenic and non-angiogenic treatment regimens.

The data presented here highlight the importance of appropriate model selection in the evaluation of any novel therapy. Sonic Hedgehog MB tumors initiated in MCre:*Ptch1* GEMM present with a completely intact BBTB, similar to previously described *Smo:Smo* SHH MB GEMM tumors.[17] This intact setting recapitulates the status of the BBB observed in patients diagnosed with Gp4 MB,[15] highlighting not only the importance of GEMM models in addressing MB recurrence, but that GEMM models are essential for therapeutic development for Gp4 MB subgroup tumors. In contrast, PDOX and transplanted ortho-MCre:*Ptch1* tumors display heterogeneous BBTB disruption. These models are representative of the BBTB phenotype observed in patients with Gp3 and SHH MB[15,16] and are histologically and genomically representative of the human tumors of which they were derived.[6] However, our findings clearly show that caution is required given the prolific use of PDOX models for the assessment of new therapeutic approaches for MB. We propose that in addition to evaluating whether or not a particular agent extends the survival of tumor-bearing mice, that it is imperative to investigate successful distribution of an agent across regions of a tumor with intact vasculature and/or assessment in tumors with an entirely intact BBTB, such as those observed in GEMM, is crucial for realistic translation into the clinic and ultimately improving patient prognosis.

Supplementary Material

Supplementary material is available at *Neuro-Oncology* online.

Keywords

blood-brain barrier | magnetic resonance imaging | medulloblastoma | patient-derived xenograft models | vasculature

Funding

This work was supported by the Kids Cancer Project, Brainchild, Children's Hospital Foundation, and the Cure Brain Cancer Foundation. This work was also supported by an NHMRC grant (GNT1164945) to C.S.B.

Acknowledgments

We thank Dr. Cameron Snell and Dr. James Conway for histopathology support and assistance. The HIF1A antibody was kindly gifted by A/Prof. Paul Timpson (Garvan Medical Research Institute).

Conflict of interest statement. The authors declare no competing financial interests

Authorship statement. Designed research: L.A.G., S.P., and B.J.W. Performed research: L.A.G., S.P., A.M., P.J., C.S.B., and C.B. Data analysis: L.A.G., S.P., A.K.L., M.K., and C.S.B. Data interpretation: L.A.G., S.P., A.K.L., and C.S.B. Manuscript preparation: L.A.G., S.P., C.A., C.B., and B.J.W.

References

1. Northcott PA, Robinson GW, Kratz CP, et al. Medulloblastoma. *Nat Rev Dis Primers.* 2019;5(1):11.
2. Cavalli FMG, Remke M, Rampasek L, et al. Intertumoral heterogeneity within medulloblastoma subgroups. *Cancer Cell.* 2017;31(6):737–754. e736.
3. Gajjar A, Pizer B. Role of high-dose chemotherapy for recurrent medulloblastoma and other CNS primitive neuroectodermal tumors. *Pediatr Blood Cancer.* 2010;54(4):649–651.
4. Gould SE, Junttila MR, de Sauvage FJ. Translational value of mouse models in oncology drug development. *Nat Med.* 2015;21(5):431–439.
5. Roussel MF, Stripay JL. Modeling pediatric medulloblastoma. *Brain Pathol.* 2020;30(3):703–712.
6. Brabetz S, Leary SES, Gröbner SN, et al. A biobank of patient-derived pediatric brain tumor models. *Nat Med.* 2018;24(11):1752–1761.
7. Cook Sangar ML, Genovesi LA, Nakamoto MW, et al. Inhibition of CDK4/6 by palbociclib significantly extends survival in medulloblastoma patient-derived xenograft mouse models. *Clin Cancer Res.* 2017;23(19):5802–5813.
8. Obermeier B, Daneman R, Ransohoff RM. Development, maintenance and disruption of the blood-brain barrier. *Nat Med.* 2013;19(12):1584–1596.
9. Zhao Z, Nelson AR, Betsholtz C, Zlokovic BV. Establishment and dysfunction of the blood-brain barrier. *Cell.* 2015;163(5):1064–1078.
10. Hay M, Thomas DW, Craighead JL, Economides C, Rosenthal J. Clinical development success rates for investigational drugs. *Nat Biotechnol.* 2014;32(1):40–51.
11. Cao Y, Sundgren PC, Tsien CI, Chenevert TT, Junck L. Physiologic and metabolic magnetic resonance imaging in gliomas. *J Clin Oncol.* 2006;24(8):1228–1235.
12. Cha S. Neuroimaging in neuro-oncology. *Neurotherapeutics.* 2009;6(3):465–477.
13. Oberoi RK, Parrish KE, Sio TT, Mittapalli RK, Elmquist WF, Sarkaria JN. Strategies to improve delivery of anticancer drugs across the blood-brain barrier to treat glioblastoma. *Neuro Oncol.* 2016;18(1):27–36.
14. Barajas RF Jr, Phillips JJ, Parvataneni R, et al. Regional variation in histopathologic features of tumor specimens from treatment-naive glioblastoma correlates with anatomic and physiologic MR imaging. *Neuro Oncol.* 2012;14(7):942–954.
15. Perreault S, Ramaswamy V, Achrol AS, et al. MRI surrogates for molecular subgroups of medulloblastoma. *AJNR Am J Neuroradiol.* 2014;35(7):1263–1269.
16. Łastowska M, Jurkiewicz E, Trubicka J, et al. Contrast enhancement pattern predicts poor survival for patients with non-WNT/SHH medulloblastoma tumours. *J Neurooncol.* 2015;123(1):65–73.
17. Girard E, Ditzler S, Lee D, et al. Efficacy of cabazitaxel in mouse models of pediatric brain tumors. *Neuro Oncol.* 2015;17(1):107–115.
18. Phoenix TN, Patmore DM, Boop S, et al. Medulloblastoma genotype dictates blood brain barrier phenotype. *Cancer Cell.* 2016;29(4):508–522.
19. Tofts PS, Kermode AG. Measurement of the blood-brain barrier permeability and leakage space using dynamic MR imaging. 1. Fundamental concepts. *Magn Reson Med.* 1991;17(2):357–367.
20. Guo L, Zhang H, Hou Y, Wei T, Liu J. Plasmalemma vesicle-associated protein: a crucial component of vascular homeostasis. *Exp Ther Med.* 2016;12(3):1639–1644.
21. Ellis T, Smyth I, Riley E, et al. Patched 1 conditional null allele in mice. *Genesis.* 2003;36(3):158–161.
22. Schüller U, Zhao Q, Godinho SA, et al. Forkhead transcription factor FoxM1 regulates mitotic entry and prevents spindle defects in cerebellar granule neuron precursors. *Mol Cell Biol.* 2007;27(23):8259–8270.
23. Wenger RH, Stiehl DP, Camenisch G. Integration of oxygen signaling at the consensus HRE. *Sci STKE.* 2005;2005(306):re12.
24. Zerbino DR, Achuthan P, Akanni W, et al. Ensembl 2018. *Nucleic Acids Res.* 2018;46(D1):D754–D761.
25. Felix R, Schörner W, Laniado M, et al. Brain tumors: MR imaging with gadolinium-DTPA. *Radiology.* 1985;156(3):681–688.
26. Tofts PS, Brix G, Buckley DL, et al. Estimating kinetic parameters from dynamic contrast-enhanced T(1)-weighted MRI of a diffusable tracer: standardized quantities and symbols. *J Magn Reson Imaging.* 1999;10(3):223–232.
27. Warso MA, Maniotis AJ, Chen X, et al. Prognostic significance of periodic acid-Schiff-positive patterns in primary cutaneous melanoma. *Clin Cancer Res.* 2001;7(3):473–477.
28. Maniotis AJ, Folberg R, Hess A, et al. Vascular channel formation by human melanoma cells in vivo and in vitro: vasculogenic mimicry. *Am J Pathol.* 1999;155(3):739–752.
29. Wimmer I, Tietz S, Nishihara H, et al. PECAM-1 stabilizes blood-brain barrier integrity and favors paracellular T-cell diapedesis across

the blood-brain barrier during neuroinflammation. *Front Immunol.* 2019;10:711.

30. di Tomaso E, Capen D, Haskell A, et al. Mosaic tumor vessels: cellular basis and ultrastructure of focal regions lacking endothelial cell markers. *Cancer Res.* 2005;65(13):5740–5749.
31. Hashizume H, Baluk P, Morikawa S, et al. Openings between defective endothelial cells explain tumor vessel leakiness. *Am J Pathol.* 2000;156(4):1363–1380.
32. Carson-Walter EB, Hampton J, Shue E, et al. Plasmalemmal vesicle associated protein-1 is a novel marker implicated in brain tumor angiogenesis. *Clin Cancer Res.* 2005;11(21):7643–7650.
33. Krock BL, Skuli N, Simon MC. Hypoxia-induced angiogenesis: good and evil. *Genes Cancer.* 2011;2(12):1117–1133.
34. Sowter HM, Raval RR, Moore JW, Ratcliffe PJ, Harris AL. Predominant role of hypoxia-inducible transcription factor (Hif)-1alpha versus Hif-2alpha in regulation of the transcriptional response to hypoxia. *Cancer Res.* 2003;63(19):6130–6134.
35. Kola I, Landis J. Can the pharmaceutical industry reduce attrition rates? *Nat Rev Drug Discov.* 2004;3(8):711–715.
36. Brighi C, Puttick S, Rose S, et al. The potential for remodelling the tumour vasculature in glioblastoma. *Adv Drug Deliv Rev.* 2018;136–137: 49–61.
37. Sarkaria JN, Hu LS, Parney IF, et al. Is the blood-brain barrier really disrupted in all glioblastomas? A critical assessment of existing clinical data. *Neuro Oncol.* 2018;20(2):184–191.
38. Ramaswamy V, Remke M, Bouffet E, et al. Recurrence patterns across medulloblastoma subgroups: an integrated clinical and molecular analysis. *Lancet Oncol.* 2013;14(12):1200–1207.
39. Hillen F, Griffioen AW. Tumour vascularization: sprouting angiogenesis and beyond. *Cancer Metastasis Rev.* 2007;26(3-4):489–502.
40. Thompson EM, Keir ST, Venkatraman T, et al. The role of angiogenesis in group 3 medulloblastoma pathogenesis and survival. *Neuro Oncol.* 2017;19(9):1217–1227.
41. Wang SY, Yu L, Ling GQ, et al. Vasculogenic mimicry and its clinical significance in medulloblastoma. *Cancer Biol Ther.* 2012;13(5):341–348.
42. van der Schaft DW, Seftor RE, Seftor EA, et al. Effects of angiogenesis inhibitors on vascular network formation by human endothelial and melanoma cells. *J Natl Cancer Inst.* 2004;96(19):1473–1477.
43. Seftor EA, Meltzer PS, Schatteman GC, et al. Expression of multiple molecular phenotypes by aggressive melanoma tumor cells: role in vasculogenic mimicry. *Crit Rev Oncol Hematol.* 2002;44(1):17–27.
44. Angara K, Borin TF, Rashid MH, et al. CXCR2-expressing tumor cells drive vascular mimicry in antiangiogenic therapy-resistant glioblastoma. *Neoplasia.* 2018;20(10):1070–1082.